Desalination and Water Treatment
www.deswater.com

doi:10.5004/dwt.2020.26244

206 (2020) 297–306
December

Effective adsorption Ag(I) onto triethylenetetramine-modified chitosan beads: adsorption equilibrium, kinetic, and thermodynamic studies

Guoquan Sun, Xiaohuan Tang, Limin Zhou*, Zhirong Liu, Zhanggao Le*, Guolin Huang

State Key Laboratory for Nuclear Resources and Environment, East China University of Technology, 418 Guanglan Road, 330013 Nanchang, China, emails: minglzh@sohu.com (L. Zhou), zhgle@ecut.edu.cn (Z. Le), 153620125@qq.com (G. Sun), xhtang727@sohu.com (X. Tang), zhrliu@ecut.edu.cn (Z. Liu), guolinhuang@sina.com (G. Huang)

Received 9 February 2020; Accepted 14 June 2020

ABSTRACT

The increasing heavy metal pollution caused by industrial wastewater has posed serious environmental concerns, and the removal of heavy metals such as silver becomes an urgent issue to be solved currently. In this research, novel functionalized chitosan beads were prepared by grafting of triethylenetetramine onto chitosan beads. Compared to unmodified chitosan, the triethylenetetramine-modified chitosan (CS-TA) exhibited both higher adsorption capacity and better selectivity for Ag(I) adsorption due to the introduction of amino/amine groups which has a high affinity for Ag(I). The influences of pH, sorbent dose, contact time Ag(I) concentration, and co-existed ions on Ag(I) adsorption were investigated. The adsorption kinetics could be fitted by pseudo-second-order model, whereas the adsorption isotherms could be described by the Langmuir model, indicating that chemisorption is the main mechanism for Ag(I) adsorption. The maximum adsorption capacity reached 419.8 mg/g at pH 5.0 and 298 K. The thermodynamic parameters suggest that the Ag(I) adsorption is endothermic and spontaneous. This work demonstrated that CS-TA exhibited superior performance for Ag(I) removal from aqueous solution due to its good hydrophilicity, high adsorption capacity, and fast kinetic rate, thus it could be potentially applied in wastewater treatment.

Keywords: Adsorption; Chitosan; Silver; Triethylenetetramine

1. Introduction

The environment pollution caused by heavy metal wastewater has become a serious problem due to the rapid development of electroplating, metal alloy, and photographic industries. Silver is widely used in industrial production due to its excellent photosensitivity, malleability, thermal/electrical conductivity, and antimicrobial properties. A huge amount of silver has entered into the environment through the discharge of industrial effluents. The removal of silver from wastewater has become an important concern due to its toxicity to human being and other living organisms [1].

Several physical, chemical, and biological processes have been developed for the removal/separation of Ag(I) ions. However, most of the methods suffer from their meager specificity or high cost. Alternatively, adsorption [2,3] has become a very efficient method for the recovery of metal ions (especially for the removal of metal ions with low concentration) from effluents due to its low cost and high efficiency. Many low-cost sorbents have been developed for silver removal, including clinoptilolite [1], chitosan/bamboo charcoal [4], expanded perlite [5], valonia tannin resin [6], biomass and bacterial biosorbents [7,8]. However, most of the sorbents suffer from their low adsorption capacities or selectivity, which limit their practical applications for wastewater treatment. It was reported that different adsorption mechanisms (such as ion-exchange, electrostatic attraction, and complexation) could be involved in metal adsorption,

* Corresponding authors.

depending on pH, metal speciation, solution composition, and surface charge of sorbents [9].

Chitosan is the second most abundant natural biopolymer (next to cellulose). The hydroxyl and amine groups of chitosan could act as chelation sites for the effective adsorption of metal ions [9,10]. The chemical modification of chitosan sorbents could improve their adsorption properties for metal ions. The modification generally occurs on the hydroxyl and amine groups of chitosan and this process can be easily conducted [11]. Chitosan-based resins have been proved to be very promising materials for the adsorption of heavy metal ions and organic pollutants [12]. The functionalization of new adsorptive groups on chitosan backbone could introduce new adsorption sites, change adsorption mechanism, and enhance adsorption capacity or selectivity [11,13]. The amine-containing agents were frequently used for sorbent modification to improve its adsorption performance for metal ions [9,13].

In this work, triethylenetetramine (which bears chelating amine moieties) was used for the chemical modification of chitosan beads. The lone pairs of N on amine groups could act as Lewis bases for binding metal ions (Lewis acids) The obtained sorbent was characterized by different methods such as elemental analysis, Fourier transform infrared (FT-IR), and scanning electron microscopy (SEM). The adsorption isotherms, kinetics, and thermodynamics for Ag(I) adsorption were investigated and the corresponding parameters were obtained. These parameters are important for scaling up of the process for Ag(I) adsorption from wastewater.

2. Material and methods

2.1. Materials

Chitosan (degree of deacetylation: 90%, molecular weight: 2,000–300,000 g/mol), triethylenetetramine, CH_3COOH, ethanol, and $AgNO_3$ with A.R. grade are the products from Sinopharm Chemical Reagent Co., Ltd., (Ningbo Road, Shanghai, China). Ag(I) stock solution (500 mg/L) was prepared by dissolving an appropriate amount of $AgNO_3$ in Milli-Q water. The stock solution was then diluted to the working solution with specific concentration for adsorption.

2.2. Preparation of sorbents

1.0 g chitosan was dissolved in 50 mL of CH_3COOH solution (20% w/w). The chitosan solution was then dropwisely added into 1.0 M NaOH solution to obtain chitosan hydrogel beads. The beads were filtered and then crosslinked by reacting with 20 mL of 0.1 M epichlorohydrin (in water/ethanol (1:1 v/v) solution) at 60°C under stirring and reflux for 2 h. After crosslinking, the chitosan beads (i) were filtered and extensively washed with deionized water to remove residual reagents.

The chitosan beads (i) obtained above were dispersed in 50 mL of water/ethanol (1:1 v/v) solution and 5 mL of epichlorohydrin was added to the suspension. The mixture was heated at 60°C under agitation and reflux for 4 h. After reaction, the beads (ii) were filtered and washed with ethanol and deionized water to remove unreacted epichlorohydrin.

The beads (ii) were redispersed in 60 mL water/ethanol (1:1 v/v) solution and 6 mL of triethylenetetramine was added. The mixture was heated at 80°C under agitation and reflux for 12 h. After the reaction, the final product (triethylenetetramine-modified chitosan beads, CS-TA) was filtered, extensively washed with ethanol and deionized water, and finally dried at vacuum for overnight.

The synthesis of CS-TA is shown in Fig. 1.

2.3. Characterization of the sorbents

The SEM images of the dried sorbents were collected on a Leica Cambridge S360 SEM. The CS-TA beads were fixed on the sample stage with conductive adhesive to observe their microscopic morphology. The morphology of the wet CS-TA beads after Ag(I) adsorption were also observed by the optical microscopy. FT-IR spectra for analyzing the functional groups were measured on a Nicolet, Magna-550 spectrometer. The zeta potential measurements were performed by using a DT-1200 zeta potential analyzer.

The amine content of the sorbent was determined by a volumetric method [9]: 100 mg of sorbent was mixed with 30 mL HCl solution (0.05 M) and stirred for 15 h. The residual HCl concentration was estimated by titration using NaOH solution (0.05 M). The amine content was calculated by the following equation:

$$\text{Amine content}\left(\text{mmol/g}\right)=\left(M_1-M_2\right)\times 30/0.1 \tag{1}$$

where M_1 and M_2 are the initial and final HCl concentration (M), respectively.

2.4. Adsorption experiments

The adsorption experiments were performed by shaking 10 mg of dry-based beads (which are immersed in deionized water for 1 h before adsorption) with 50 mL of Ag(I) solution at specific pH, 150 rpm, and 298 K (except for isotherms) for 2.5 h. The initial pH was adjusted by adding small amount of HNO_3 or NaOH solution. After adsorption equilibrium, the samples were taken through the filtration of the solution by a 0.22 μm membrane filter. Subsequently, the residual Ag(I) concentrations were determined by atomic adsorption spectroscopy (iCAP-7600 inductively coupled plasma–optical emission spectrometry (ICP-OES). Thermo-scientific, UK). For the evaluation of pH effect, the pH was less than 8.0 to avoid precipitation. The kinetic experiments were carried out at 350 mg/L of initial Ag(I) concentration and pH 5.0, and the samples were taken at specific time intervals for the analysis. For the study of isotherms, the initial pH and temperature were set at pH 5.0 and 298–318 K, respectively.

2.5. Adsorption selectivity

The Ag(I) adsorption selectivity experiments were performed on multi-component systems (10 mg/L of initial concentration for each metal) containing other cations (Cr^{3+}, Fe^{3+}, Pb^{2+}, Li^{+}, Zn^{2+}, Sr^{2+}, Ni^{2+}, Cu^{2+}, and Co^{2+}): 10 mg of dry-based beads with 50 mL multi-component solution for 3 h at

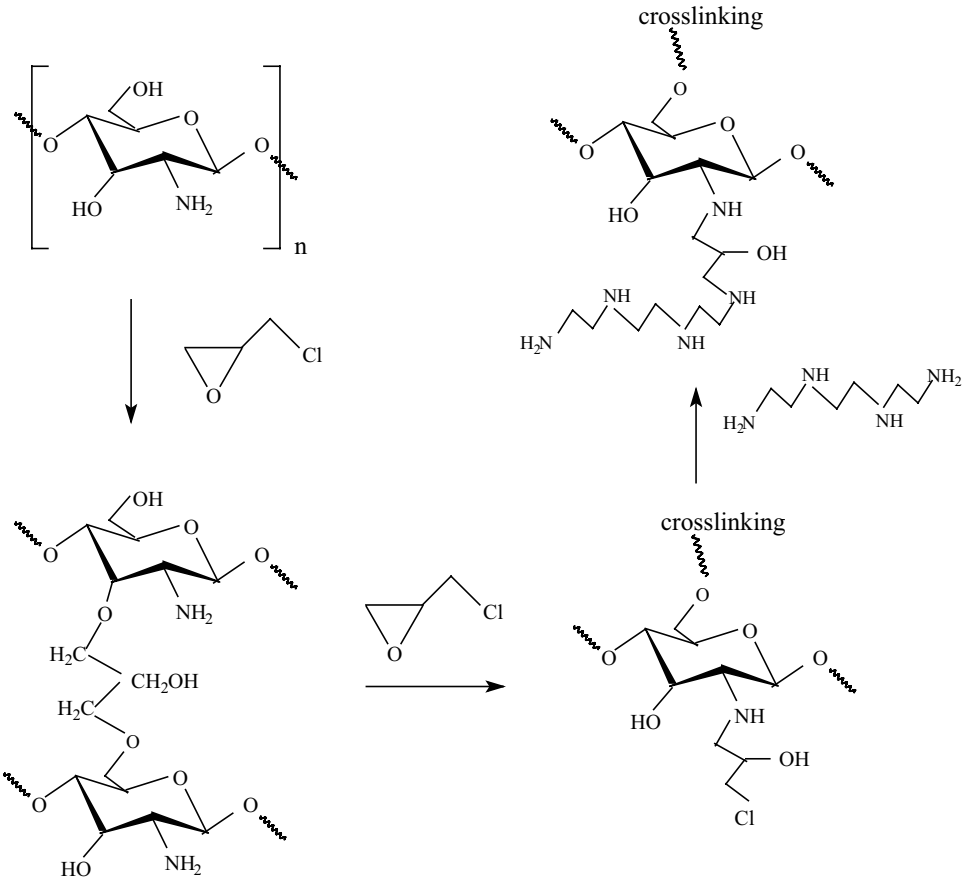

Fig. 1. Proposed route for the synthesis of CS-TA.

pH 5.0 and 298 K. After adsorption equilibrium, the residual concentrations of different metal ions were estimated using ICP-OES.

The equilibrium adsorption capacity (q_e, mg/g), the distribution coefficient (K_d) and selectivity coefficient ($S_{Ag/M}$) were determined by the following equations [14]:

$$q_e = \left(C_0 - C_e\right) \times \frac{V}{m} \tag{2}$$

$$K_d = \frac{C_0 - C_e}{C_0} \times \frac{V}{m} \tag{3}$$

$$S_{Ag/M} = \frac{K_{d,Ag}}{K_{d,M}} \tag{4}$$

where C_0 (mg/L) is the initial Ag(I) concentration; C_e (mg/L) is the equilibrium Ag(I) concentration; V is the solution volume (L), and m is the sorbent mass (g).

3. Results and discussion

3.1. Synthesize and characterization of the sorbents

The modification of chitosan by triethylenetetramine could increase the amine groups, thus it may enhance the adsorption capacity for metal ions. The chitosan-based sorbents are frequently crosslinked by glutaraldehyde to improve their chemical stability. However, the crosslinking reaction occurs on amine sites for using glutaraldehyde as the crosslinking agent, which may result in the decrease in the number of available amine groups for the complexation of metal ions. Thus, herein epichlorohydrin cross-linker was used to avoid the possible decrease in adsorptive activity of amine groups. Indeed, for epichlorohydrin cross-linker the reaction occurs with the opening of the epoxide ring, leaving a chlorine atom to make facile grafting of functional groups. The amine-containing agents such as ethylenediamine and diethylenetriamine had been frequently reported for the modification of different materials such as silica, chitosan, and polyacrylonitrile [13,15,16] to improve the adsorption performance for metal ions. Herein triethylenetetramine (which has high content of amine groups) is used as functional agent for the modification of chitosan sorbents.

The SEM images of CS-TA beads before and after adsorption are shown in Fig. 2. The CS-TA exhibits a uniform and smooth spherical shape, and the diameter range is around 0.45–0.65 mm (Fig. 2a). Meanwhile, the distribution of small cavities with the porous structure on the surface of CS-TA (Fig. 2b) is beneficial for Ag(I) entering into the inner-part of microspheres for adsorption. After adsorption, the surface of the sorbents became unsmooth (Fig. 2c), and the surface of the sorbent is uniformly covered by very small

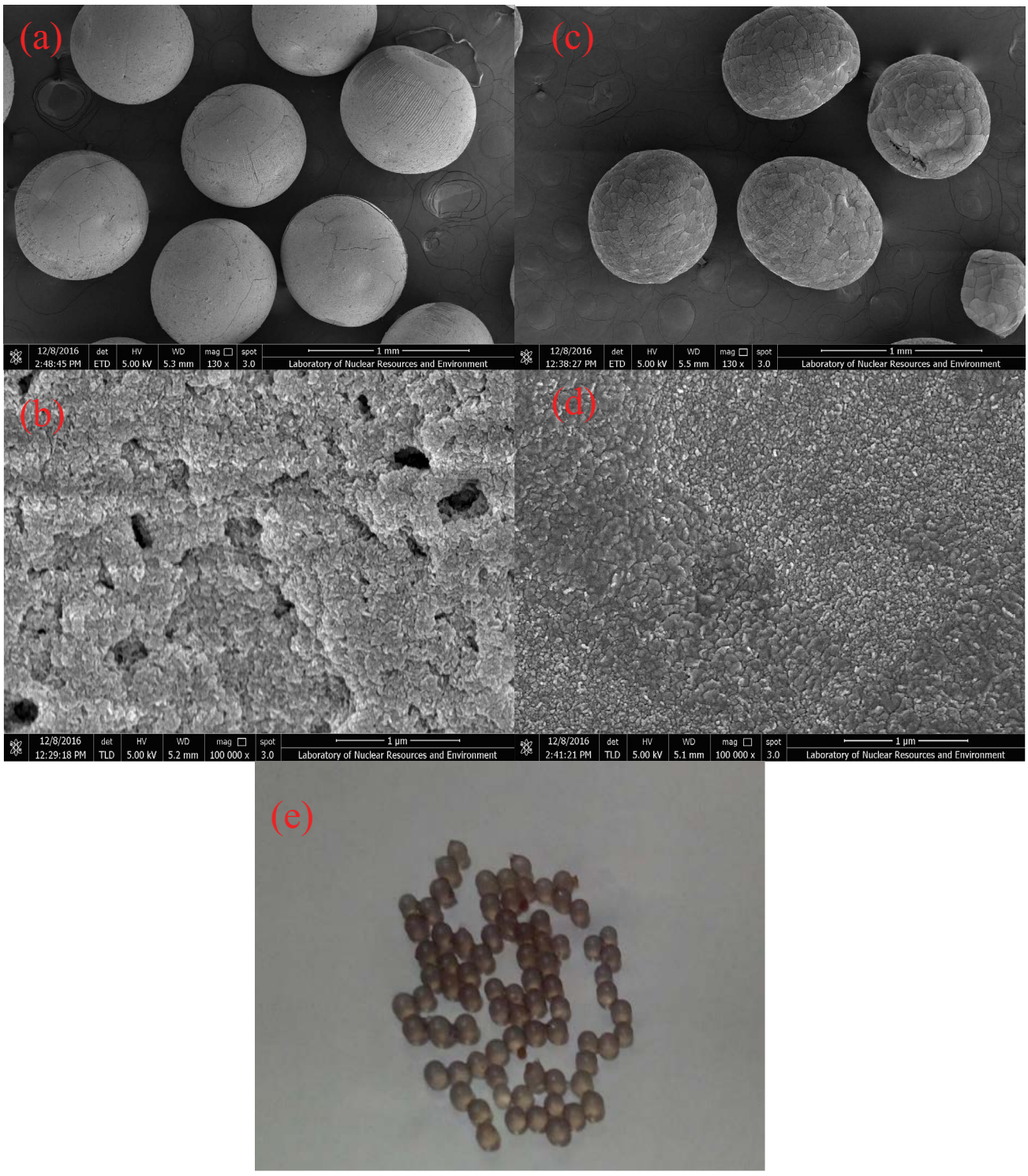

Fig. 2. SEM of (a) CS-TA beads (1 mm bar) (b) the surface of CS-TA (1 μm bar) before Ag(I) adsorption; (c) CS-TA beads (1 mm bar) (d) the surface of CS-TA (1 μm bar) after Ag(I) adsorption, and (e) the optical morphology for CS-TA wet beads after Ag(I) adsorption.

aggregates of Ag(I) species (Fig. 2d). The optical morphology (Fig. 2e) shows that CS-TA after adsorption exhibits gray–brown color due to the loading of Ag(I).

The functional groups of different products at each step for the synthesis of CS-TA was characterized by the FT-IR spectra, as shown in Fig. 3. The spectra were similar for different samples except for different relative intensity. The wide bands at 3,368 cm^{-1} or around 3,400 cm^{-1} are attributed to the combination effect of –OH groups (stretching vibration) and N–H groups (extension vibration). For CS, the peak at

1,620 cm^{-1} is assigned to amine groups, and the peaks 1,320 and 1,060 cm^{-1} are attributed to primary and secondary –OH groups (stretching vibrations); while the peaks at 1,462 and 1,365 cm^{-1} are assigned to C–O–C (stretching vibration) and –OH (bending vibration), respectively. The crosslinking of epichlorohydrin could be identified from the decrease intensity of –OH groups, while the grafting of spacer arm on crosslinked chitosan could be confirmed by the new band at 790 cm^{-1}, which is attributed to the $–CH_2–Cl$ group. After the modification of triethylenetetramine, the band at 790 cm^{-1} (related to $–CH_2–Cl$ group) it shifted to 793 cm^{-1}, whereas the intensity for the band at 1,628 cm^{-1} (related to amine group) increased [9]. The amine group for CS-TA is determined to be 5.74 mmol/g, which is much higher than the content of amine groups for CS (1.68 mmol/g).

3.2. Effect of pH

The solution pH may affect the speciation distribution of Ag(I) and its binding mechanism. The pH and the Ag(I) concentration were appropriately selected to avoid metal precipitation. For CS-TA, the final pH slightly increases by 0.17–0.48 after Ag(I) adsorption, with higher pH increase at lower pH, probably due to the protonation of active sites (the binding of H^+). As show in Fig. 4a, the Ag(I) adsorption capacity increased with pH before pH 5.0, then it slightly decreased at higher pH. The unmodified CS also shows similar trend to the CS-TA for Ag(I) adsorption. Meanwhile, the Ag(I) adsorption capacity for CS-TA is significantly higher than for the unmodified CS, owing to the introduction of amine binding sites for Ag(I) adsorption.

The results of zeta potential of CS and CS-TA are shown in Fig. 4b. The pH point of zero charge (pH_{ZPC}) of CS and CS-TA are determined to be 5.18 and 5.67, respectively. The higher zeta potential of CS-TA compared to CS is due to the chemical binding of the basic amine groups to the surface of CS-TA. Below pH_{ZPC} the sorbents are positively charged, which is unfavorable for the adsorption of positive Ag(I) ions. Meanwhile, the strong competition of protons at low pH also reduces the affinity of the sorbents for metal ions. Under acidic medium conditions, the adsorption may proceed through by ion-exchange on protonated amine groups (as shown in Eq. (4)). When the pH increases, the deprotonation of the reactive groups favors the chelation of Ag(I) ions. The amine groups have lone pair electrons and high negative electron cloud density, which are beneficial for attracting positive Ag(I) through complexation (Fig. 5). However, the slight decrease of the adsorption capacity over pH 6.0 is probably due to the formation of anion Ag(I) species ($Ag(OH)_n^{1-n}$) [4], which are unfavorable for adsorption on the negative surface of the sorbents at high pH due to electrostatic repulsion.

$$R-NH_3^+ + Ag^+ \rightarrow R-NH_2\cdot Ag^+ + H^+ \quad (5)$$

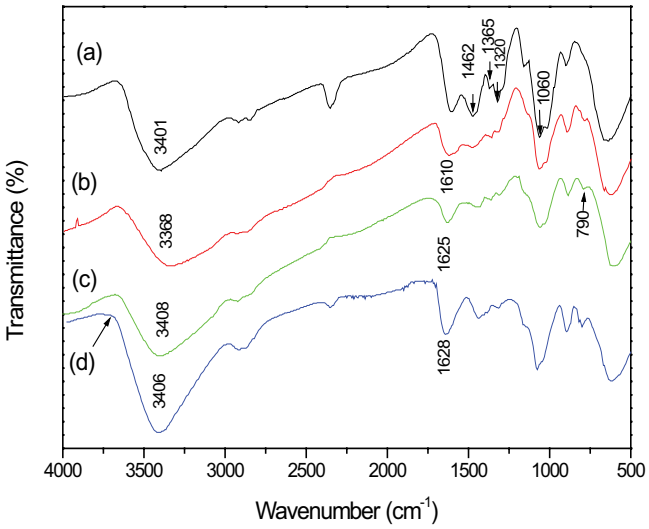

Fig. 3. FT-IR spectra of (a) CS, (b) CS cross-linked with epichlorohydrin, (c) cross-linked CS with spacer arm, and (d) CS-TA.

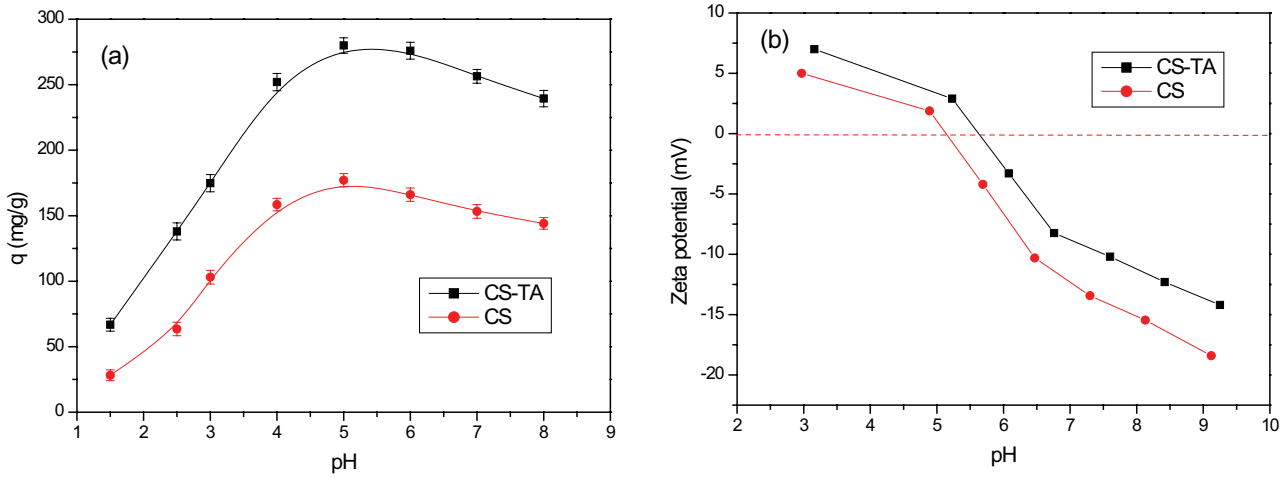

Fig. 4. (a) Effect of pH on Ag(I) adsorption (C_0 = 350 mg/L, SD (sorbent dosage) = 0.2 g/L, and T = 298 K) and (b) zeta potential of CS and CS-TA.

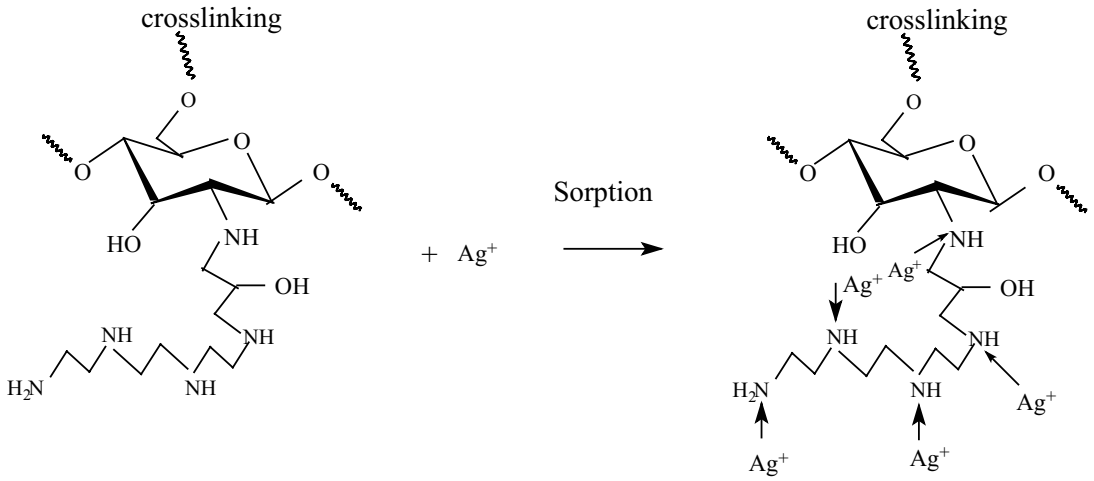

Fig. 5. Probable complexation for Ag(I) adsorption by the sorbents.

3.3. Effect of sorbent dosage

The effect of SD on Ag(I) adsorption is shown in Fig. 6. It shows that when SD is decreasing, the adsorption capacity (q_e) for Ag(I) continuously increases, especially it increases rapidly at SD < 0.4 g/L. This indicates that the sorbent is unsaturated and the Ag(I) in the solution is not enough to reach saturation. At 0.2 g/L of SD, the q_e reaches 280 mg/gL. The removal efficiency almost increased linearly with SD due to greater accessibility of binding sites. In order to achieve high adsorption capacity (close to saturated adsorption capacity) for isotherms, the sorbent dose is selected to be 0.20 g/L.

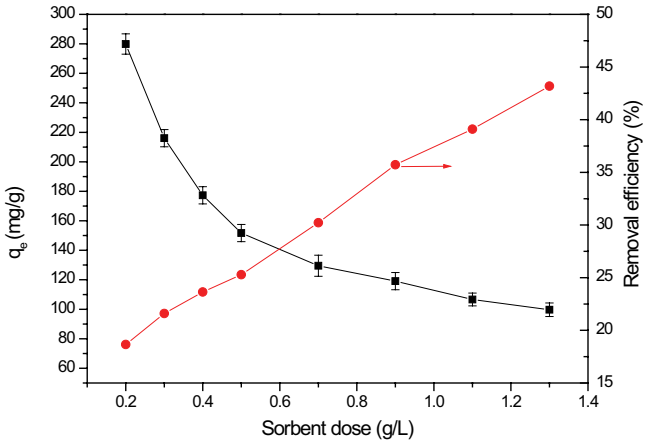

Fig. 6. Effect of sorbent dose of CS-TA on Ag(I) adsorption.

3.4. Adsorption kinetics

Fig. 7 shows the effect of contact time on Ag(I) adsorption by CS and CS-TA. The kinetic profiles are characterized by the initial fast adsorption within 40 min and the following slow adsorption until equilibrium. This can be explained by the fast decrease on the Ag(I) concentration gradient and the rapid occupation of the active sites in the initial stage, but this process becomes slow before reaching adsorption saturation, leading to the slow Ag(I) adsorption at the latter stage.

The mass transfer for adsorption could be controlled by bulk diffusion, external diffusion, intraparticle diffusion, and reaction. For a well-mixed system, the effect of external diffusion can be almost neglected [17]. To determine the rate-controlling step, the kinetic data were fitted by different kinetic models, including pseudo-first-order (PFO, Eq. (6)) [18], pseudo-second-order (PSO, Eq. (7)) [19], and intraparticle diffusion resistance (IDR, Eq. (8)) models [20]:

$$q_t = q_e\left(1 - e^{-k_1 t}\right) \tag{6}$$

$$q_t = \frac{q_e^2 k_2 t}{1 + q_e k_2 t} \tag{7}$$

$$q_t = k_{\text{int}} t^{1/2} + C \tag{8}$$

where q_t and q_e is the adsorption capacities (mg/g) for Ag(I) at contact time t (min) and at equilibrium; k_1 (1/min), k_2 (g/mg/min), and k_{int} (mg/g/min$^{0.5}$) are the rate constants for PFO, PSO, and IDR models, respectively.

The parameters for the kinetic models are summarized in Table 1. The results show that the PSO is the best for fitting the kinetic data according to the correlation coefficients. Meanwhile, the theoretical Ag(I) adsorption capacity calculated from PSO is close to the experimental value. The PSO is suitable for describing experimental data, indicating that chemisorption is the rate–determine step for Ag(I) adsorption. The PFO and PSO models were initially developed for describing homogeneous adsorption. Extrapolating these models to heterogeneous adsorption means that the rate parameters are "apparent parameters", and thus it is still hard to exclude the contribution of diffusion mechanism. It is noteworthy that although IDR model fitted worst for Ag(I) adsorption on the whole adsorption stage, this model could be fitted well with the kinetic data in the initial fast adsorption stage (results are shown). This indicates that except for chemisorption, the intraparticle diffusion also plays an important role in controlling the

kinetic rate at the initial adsorption stage. Similar results were reported in the literatures for metal ion adsorption onto the chitosan/chitosan-based resins [14,17].

3.5. Adsorption isotherms at different temperatures

Fig. 8 shows the adsorption isotherms for Ag(I) adsorption onto CS and CS-TA beads at 298–318 K. The adsorption isotherms are characterized by the progressive increase of capacity with metal concentration. The Langmuir (Eq. (9)) [21], Freundlich (Eq. (10)) [22], and Dubinin–Radushkevich (D–R, Eq. (11)) [23] models, respectively) were used to describe the isotherm adsorption data:

$$q_e = \frac{K_L q_m C_e}{1 + K_L C_e} \tag{9}$$

$$q_e = K_F C_e^{1/n} \tag{10}$$

$$q_e = q_{DR} e^{-K_{DR}\varepsilon^2} \tag{11}$$

where q_m (mg/g) is the maximum adsorption capacity for Ag(I), K_L (L/mg), and K_F (mg^{1-n} L^n/g) are constants for the Langmuir and Freundlich models, respectively; n is heterogeneous factor related to the adsorption intensity; q_{DR} and K_{DR} are the saturation adsorption capacity and the constant for D–R model, ε is the Polanyi potential: $\varepsilon = RT \ln(1 + 1/C_e)$; and E_{DR} (kJ/mol) (Eq. (12)) is the mean-free adsorption energy for per mol of sorbate [23].

$$E_{DR} = \frac{1}{\sqrt{2K_{DR}}} \tag{12}$$

The isothermal parameters for the models are listed in Table 2. This non-linear fitting results of the data using Langmuir and Freundlich models are also shown in Fig. 8. Obviously, the Langmuir model with highest R^2 values provides the best fitting results for the experimental data. The CS-TA containing the amine moiety exhibits over 50% higher adsorption capacities than CS. The higher K_L for CS-TA compared to CS beads indicate a higher affinity of CS-TA beads for Ag(I) adsorption. In addition, the $1/n$ values (0.47–0.54 for CS-TA) is less than 1, indicating that Ag(I) adsorption is favorable. The E_{DR} (8.84–9.59 kJ/mol for CS-TA) are greater than 8 kJ/mol, indicating chemisorption is the main adsorption mechanism for Ag(I) [24,25]. This is in agreement with the hypotheses of mono-layer homogeneous adsorption for the Langmuir model. This model supposes the adsorption to occur as a monolayer without interactions between adsorbed molecules and with equivalent adsorption energies (homogeneous adsorption).

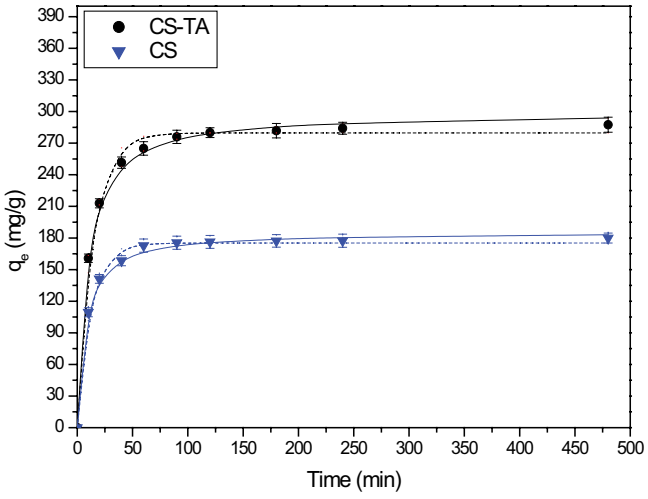

Fig. 7. Adsorption kinetic curves for the uptake of Ag(I) by CS and CS-TA (C_0 = 350 mg/L; T = 298 K, initial pH = 5.0, and SD = 0.2 g/L. The solid lines represent the PSO model and the dash lines represent the PFO model).

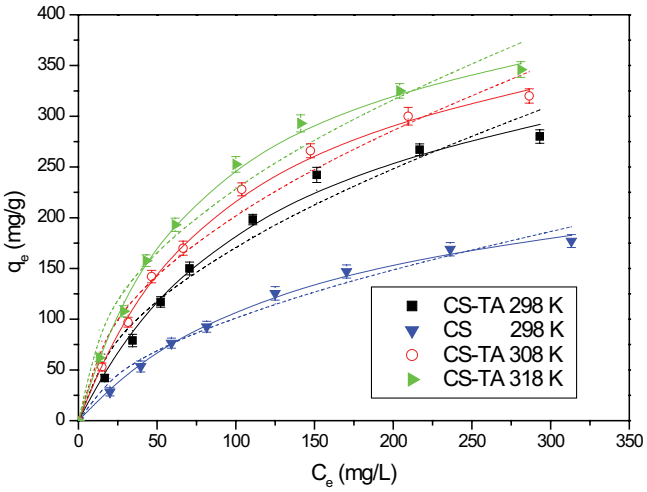

Fig. 8. Adsorption isotherms for Ag(I) adsorption on CS and CS-TA (pH = 5.0, SD = 0.2 g/L, and 298 K. The solid lines represent Langmuir model and the dash lines represent Freundlich model).

Table 1
Kinetic parameters of the adsorption of Ag(I) by CS and CS-TA

Concentration (mg/L)	PFO				PSO			RID		
	$q_{e,exp}$ (mg/g)	k_1 (1/min)	$q_{e,cal}$ (mg/g)	R^2	$k_2 \times 10^4$ (g/mg/min)	$q_{e,cal}$ (mg/g)	R^2	k_{int} (mg/g/min$^{0.5}$)	X	R^2
CS-TA	287.5	0.075	279.7	0.965	4.04	298.9	0.994	10.41	133.75	0.541
CS	179.6	0.087	175.2	0.952	8.06	185.6	0.997	6.24	88.71	0.511

Table 2
Parameters of the Langmuir and Freundlich models for Ag(I) adsorption on CS and CS-TA

Sorbent	Temperature	Langmuir			Freundlich			D–R			
		q_m (mg/g)	$K_L \times 10^3$ (L/mg)	R^2	K_F (mg^{1-n}L^n/g)	n	R^2	q_{DR} (mg/g)	$K_{DR} \times 10^9$ (J^2/mol^2)	E (kJ/mol)	R^2
CS-TA	298 K	419.8	7.79	0.994	14.41	1.86	0.967	112.9	6.39	8.84	0.971
	308 K	443.2	9.73	0.998	20.26	1.99	0.976	119.6	5.88	9.22	0.980
	318 K	455.9	12.03	0.998	26.83	2.14	0.974	128.8	5.43	9.59	0.977
CS	298 K	270.8	6.61	0.997	7.98	1.81	0.978	75.6	6.65	8.67	0.982

It should be noted that the mathematical fitting of the data may help in interpreting the metal binding mechanism, but it does not definitely verify the model hypotheses.

As shown in Fig. 8, the Ag(I) adsorption amounts at equilibrium increased with temperature, indicating that the adsorption process is endothermic. The adsorption sites with higher energy could binding Ag(I) at higher temperatures, leading to an increase of adsorption capacity. The Gibbs free energy change ($\Delta G°$), enthalpy change ($\Delta H°$), and entropy change ($\Delta S°$) could be calculated from the following equations [25]:

$$\ln K_L = \frac{-\Delta H°}{RT} + \frac{\Delta S°}{R} \tag{13}$$

$$\Delta G° = \Delta H° - T\Delta S° \tag{14}$$

where K_L is the Langmuir constant obtained from isotherms and T is Kelvin temperature. The plotting line of ln K_L against 1/T is shown in Fig. 9. From the slope and the intercept of the line, the $\Delta H°$ and $\Delta S°$ values were obtained. The thermodynamics parameters are provided in Table 3. The positive value of $\Delta H°$ (=17.11 kJ/mol) confirms the endothermic nature of Ag(I) adsorption onto CS-TA. The negative $\Delta G°$ (= –16.69 to –18.96 kJ/mol) indicates that Ag(I) adsorption is spontaneous, and this value becomes more negative at higher temperature, indicating more favourable Ag(I) adsorption at higher temperature. The positive $\Delta S°$ (=113.42 J/mol K) means the increase in the randomness of the system after adsorption, probably related to the removal of water shell for the hydrated Ag(I) ions.

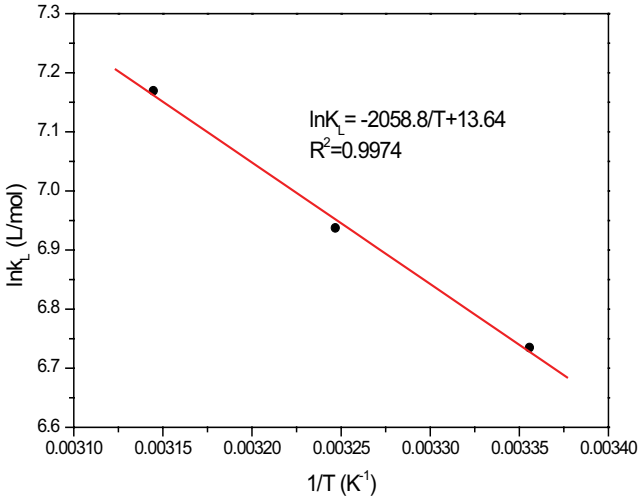

Fig. 9. Fitting line of van't Hoff equation for Ag(I) adsorption on CS-TA.

Table 3
Thermodynamic parameters for adsorption of Ag(I) by CS-TA

$\Delta H°$ (kJ/mol)	$\Delta S°$ (J/mol K)	$\Delta G°$ (kJ/mol)			R^2
		298 K	308 K	318 K	
17.11	113.42	–16.69	–17.83	–18.96	0.9974

3.6. Adsorption of Ag(I) from the simulated solution

The adsorption selectivity was investigated by the adsorption of Ag(I) from the simulated solution containing other co-existed cations (some of them exist naturally along with silver enriched ores). The selectivity coefficients ($S_{Ag/M}$) are shown in Fig. 10. The CS-TA has excellent selectivity for Ag(I) ions, due to the introduction of specific active sites, that is, amine groups which could coordinate with Ag(I) ions. Especially, CS-TA is very efficient for the selective separation of Ag(I) from Cd(II), Cr(III), Cu(II), Mn(II), and Ni(II) ions, and the $S_{Ag/M}$ values range from 278 to 762. The selective adsorption of Ag(I) from the system of mixed metal ions is attributed to the relatively stronger complexation between Ag(I) ions with the amine groups of CS-TA. The Ag(I) ions more easily provided empty orbits for the lone pair of electrons in nitrogen atoms of the active groups, and this may be the reason why Ag(I) was preferentially removed by CS-TA [4,11,12].

3.7. Comparison with other sorbents

The comparison of CS-TA with other reported sorbents [26–29] is shown in Table 4. The CS-TA has relatively high adsorption capacity (q_m) for Ag(I), which is much higher than the q_m values of carbon and natural biomass. It should be mentioned that except for high adsorption capacity, CS-TA also presents excellent adsorption selectivity for Ag(I), and this is very important for the recovery of silver from a realistic wastewater system which contains multiple co-existed ions. However, the comparison of the adsorption

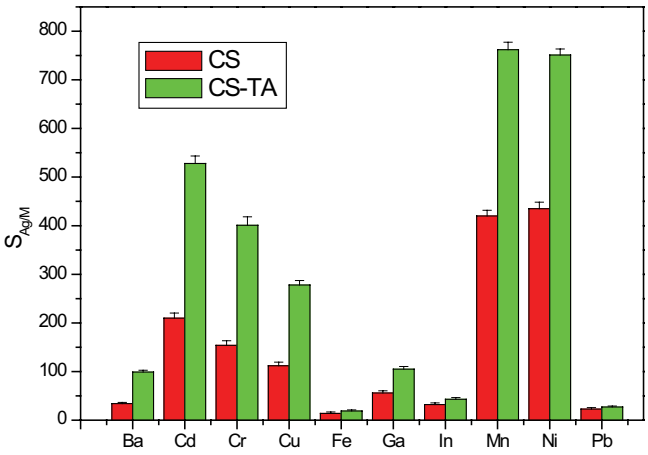

Fig. 10. Adsorption selectivity of Ag(I) in the presence of different co-existing ions.

Table 4
Comparison of the Ag(I) adsorption capacities of different sorbents

Sorbent	pH	q_m (mg/g)	Reference
Chitosan	6.0	42.2	[26]
Poly(o-phenylenediamine) microparticles	5.0	533.3	[27]
Carbon sorbents	5.0	114.5	[28]
Myxococcus xanthus biomass	6.0	17	[29]
Triethylenetetramine-modified chitosan beads (CS-TA)	5.0	419.8	This work
Chitosan beads (CS)	5.0	270.8	

Table 5
Repeated adsorption of Ag(I) ions by CS-TA (adsorption conditions: C_0 = 350 mg/L, pH 5.0, and 298 K)

Cycle number	Adsorption capacity (mg/g)
1	280
2	263
3	255
4	247

selectivity of these resins is difficult since only the data of adsorption capacities are available in most literatures. The results in this work have demonstrated that CS-TA has the advantages of high adsorption capacity and excellent adsorption selectivity for Ag(I) adsorption.

3.8. Desorption and regeneration of the sorbents

After usage, the beads could also be desorbed and reused. When 0.20 g of Ag(I)-loaded CS-TA Ag(I) initial concentration 350 mg/L for adsorption) was eluented with 10 mL of 0.1, 0.2, 0.5, and 1.0 M HNO_3, the desorption efficiency reached 52%, 73%, 91%, and 95%, respectively. Using 0.5 M HNO_3 as the eluent, the desorbed CS-TA beads could be reused four adsorption–desorption cycles without significant decrease in the adsorption capacity (q_e decreased by less than 12%), as shown in Table 5. These results indicated no appreciable loss in activity over at least four cycles for CS-TA beads.

4. Conclusions

The triethylenetetramine-modified chitosan beads (CS-TA) exhibits relatively high capacity, fast kinetic as well as excellent slectivity for Ag(I) adsorption, since the modification with triethylenetetramine for the biopolymer introduced amine groups, which imparted selective and specific properties for the material. Compared to CS, the CS-TA has much higher adsorption capacity for Ag(I) (q_m = 419.8 mg/g). The good fitting of uptake kinetics by PSO suggests a chemisorption mechanism, which is in agreement with the mono-layer chemisorption hypothesis of the Langmuir model. Meanwhile, the E_{DR} values obtained from the IDR model are larger than 8 kJ/mol, which also indicates the chemisorption mechanism. The amine groups are the main adsorption sites, which could bind Ag(I) through the ion-exchange or chelating mechanism. As a novel biosorbent, CS-TA hydrogel is cost-effective, highly efficient, and reusable, and it could be potentially used in the processing and enrichment of Ag(I) other precious metals.

Acknowledgments

The financial supports from National Natural Science Foundation (21667001, 21866002, 21866005, 21706028, and 21866006) and the Key Research and Development Project of Jiangxi Province (20192BBH80011) were acknowledged.

References

[1] M. Akgül, A. Karabakan, O. Acar, Y. Yürüm, Removal of silver(I) from aqueous solutions with clinoptilolite, Microporous Mesoporous Mater., 94 (2006) 99–104.
[2] W.W. Ngah, M.M. Hanafiah, Removal of heavy metal ions from wastewater by chemically modified plant wastes as sorbents: a review, Bioresour. Technol., 99 (2008) 3935–3948.
[3] I. Yanti, W.F. Winata, M. Anugrahwati, Utilization of hydrotalcite modified with 3,4,5-trihydroxybenzoic acid for the treatment of silver-containing wastewater, IOP Conf. Ser.: Mater. Sci. Eng., 349 (2018) 12–28.
[4] W. Nitayaphat, T. Jintakosol, Removal of silver(I) from aqueous solutions by chitosan/bamboo charcoal composite beads, J. Cleaner Prod., 87 (2015) 850–855.
[5] H. Ghassabzadeh, A. Mohadespour, M. Torab-Mostaedi, P. Zaheri, M.G. Maragheh, H. Taheri, Adsorption of Ag, Cu and Hg from aqueous solutions using expanded perlite, J. Hazard. Mater., 177 (2010) 950–955.
[6] M. Yurtsever, A. Şengl, Adsorption and desorption behavior of silver ions onto valonia tannin resin, Trans. Nonferrous Met. Soc. China, 22 (2012) 2846–2854.
[7] S. Zafar, N. Khalid, M.L. Mirza, Potential of rice husk for the decontamination of silver ions from aqueous media, Sep. Sci. Technol., 47 (2012) 1793–1801.
[8] K. Vijayaraghavan, Y.S. Yun, Bacterial biosorbents and bioadsorption, Biotechnol. Adv., 26 (2008) 266–291.
[9] L. Zhou, J. Ouyang, Z. Liu, G. Huang, Y. Wang, Z. Li, A.A. Adesina, Highly efficient adsorption of U(VI) from aqueous solution using amino/amine-functionalized magnetic

mesoporous silica nanospheres, J. Radioanal. Nucl. Chem., 319 (2019) 987–995.
[10] J. Ouyang, Y. Wang, T. Li, L. Zhou, Z. Liu, Immobilization of carboxyl-modified multiwalled carbon nanotubes in chitosan-based composite membranes for U(VI) adsorption, J. Radioanal. Nucl. Chem., 317 (2018) 1419–1428.
[11] S.K. Shukla, A.K. Mishra, O.A. Arotiba, B.B. Mamba, Chitosan-based nanomaterials: a state-of-the-art review, Int. J. Biol. Macromol., 59 (2013) 46–58.
[12] R. Jayakumar, M. Prabaharan, R.L. Reis, J. Mano, Graft copolymerized chitosan-present status and applications, Carbohydr. Polym., 62 (2005) 142–158.
[13] Y. Liu, L. Yuan, Y. Yuan, J. Lan, Z. Li, Y. Feng, W. Shi, A high efficient adsorption of U(VI) from aqueous solution using amino-functionalized SBA-15, J. Radioanal. Nucl. Chem., 292 (2012) 803–810.
[14] L. Zhou, C. Shang, Z. Liu, G. Huang, A.A. Adesina, Selective adsorption of uranium(VI) from aqueous solutions using the ion-imprinted magnetic chitosan resins, J. Colloid Interface Sci., 366 (2012) 165–172.
[15] M.G. Mahfouz, A.A. Galhoum, N.A. Gomaa, S.S. Abdel-Rehem, A.A. Atia, T. Vincent, E. Guibal, Uranium extraction using magnetic nano-based particles of diethylenetriamine-functionalized chitosan: equilibrium and kinetic studies, Chem. Eng. J., 262 (2015) 198–209.
[16] G.R. Kiani, H. Sheikhloie, N. Arsalani, Heavy metal ion removal from aqueous solutions by functionalized polyacrylonitrile, Desalination, 269 (2011) 266–270.
[17] A. Benettayeb, E. Guibal, A. Morsli, R. Kessas, Chemical modification of alginate for enhanced adsorption of Cd(II), Cu(II), and Pb(II), Chem. Eng. J., 316 (2017) 704–714.
[18] S. Lagergreen, Zur theorie der sogenannten adsorption geloster stoffe, Kungl. Svens. Vetenskapsakad. Handl., 24 (1898) 1–39.
[19] Y.S. Ho, G. Mckay, Adsorption of dye from aqueous solution by peat, Chem. Eng. J., 70 (1998) 115–124.
[20] C. Nemasivayam, R.T. Yamuna, Adsorption of direct red 12B by biogas residual slurry: equilibrium and rate processes, Environ. Pollut., 89 (1995) 1–7.
[21] I. Langmuir, The adsorption of gases on plant surfaces of glass, mica and platinum, J. Am. Chem. Soc., 40 (1918) 1361–1403.
[22] H.M.F. Freundlich, Uber die adsorption in losungen, Z. Phys. Chem., 57 (1906) 385–470.
[23] A.A. Galhoum, A.A. Atia, M.G. Mahfouz, S.T. Abdel-Rehem, N.A. Gomaa, T. Vincent, E. Guibal, Dy(III) recovery from dilute solutions using magnetic-chitosan nano-based particles grafted with amino acids, J. Mater. Sci., 50 (2015) 2832–2848.
[24] T. Li, Q. Chen, L. Zhou, Z. Le, Y. Wang, Z. Liu, A.A. Adesina, Efficient adsorption of Th(IV) from aqueous solutions onto magnetic chitosan nano-particles functionalized with alanine and valine, J. Radioanal. Nucl. Chem., 314 (2017) 1083–1093.
[25] L. Zhou, Z. Li, K. Zeng, Q. Chen, Y. Wang, Z. Liu, A.A. Adesina, Immobilization of in-situ formed $Ni(OH)_2$ nanoparticles in chitosan beads for efficient removal of U(VI) from aqueous solutions, J. Radioanal. Nucl. Chem., 314 (2017) 467–476.
[26] C.L. Lasko, M.P. Hurst, An investigation into the use of chitosan for the removal of soluble silver from industrial wastewater, Environ. Sci. Technol., 33(1999) 3622–3626.
[27] X.G. Li, X.L. Ma, J. Sun, M.R. Huang, Powerful reactive adsorption of silver(I) and mercury(II) onto poly(o-phenylenediamine) microparticles, Langmuir, 25 (2009) 1675–1684.
[28] O.N. Kononova, A.G. Kholmogorov, N.V. Danilenko, S.V. Kachin, Y.S. Kononov, Z.V. Dmitrieva, Adsorption of gold and silver on carbon sorbents from thiocyanate solutions, Carbon, 43 (2005) 17–22.
[29] M.L. Merroun, N.B. Omar, E. Alonso, J.M. Arias, M.T. González-Mu, Silver adsorption to myxococcus xanthus biomass, Geomicrobiol. J., 18 (2001) 183–192.